International Journal of Mass Spectrometry 287 (2009) 119–127

Contents lists available at ScienceDirect

International Journal of Mass Spectrometry

journal homepage: www.elsevier.com/locate/ijms

Wavelength dependence on the level of post-source metastable ion decay observed in infrared matrix-assisted laser desorption ionization

Edward E. Durrant, Robert S. Brown*

Department of Chemistry and Biochemistry, Utah State University, Logan, UT 84322-0300, United States

ARTICLE INFO

Article history:
Received 7 July 2008
Accepted 25 August 2008
Available online 2 September 2008

Keywords:
Infrared MALDI
PSD
Infrared
Metastable ion
Ion deceleration

ABSTRACT

The levels of post-source metastable ion decay (PSD) observed in several peptides and proteins ionized by matrix-assisted laser desorption ionization time-of-flight mass spectrometry (MALDI TOF-MS) are measured utilizing both infrared (IR) and ultraviolet (UV) desorption wavelengths. A gridless deceleration ion optic is employed to temporally separate stable analyte ions from analyte metastable neutral and ion fragments. Comparisons of the extent of PSD that is observed in UV-MALDI at 337 nm and IR-MALDI at multiple wavelengths between 2.8 and 3.0 μm are made using the same matrices and analytes. The amount of PSD observed using IR-MALDI was found to be highly dependent on the specific IR wavelength (2.8–3.0 μm) employed for desorption. IR wavelengths shorter than 2.86 μm tended to produce higher levels of PSD, while longer IR wavelengths typically produced significantly less PSD when using a number of common MALDI matrices. Relative PSD levels are quantified by determining the percentage of the neutral fragment signal intensity to the intensity of the stable singly protonated molecular species observed in decelerated MALDI spectra. These studies suggest that an analyte ion activation pathway leading to significant PSD in IR-MALDI may proceed by way of vibrational excitation of the analyte molecules during the desorption event.

1. Introduction

Matrix-assisted laser desorption ionization time-of-flight mass spectrometry (MALDI TOF-MS) has become an important analytical tool, especially in the field of proteomics for the characterization of peptides and proteins. While it has become a standard technique for many laboratories since its introduction, the underlying fundamental processes involved in MALDI are complex. Indeed, despite the two decades that have passed since its initial development, the underlying ionization mechanism remains incompletely understood and several competing models have been proposed [1–5]. Additional complications arise when MALDI using both infrared (IR-MALDI) and ultraviolet (UV-MALDI) wavelengths for desorption are included in potential ionization models. Differences in photon energies, the depth and amount of ablated sample per laser pulse and matrix effects (including physical state) need to be addressed by any unifying model. Recent comprehensive reviews summarizing the current understanding of the desorption and ionization processes in both UV-MALDI [6] and IR-MALDI [7] have appeared and suggest that a more comprehensive understanding of MALDI is beginning to emerge. While the "Lucky Survivor" model proposed by Karas [3] may eventually serve as part of a unified model for both UV-MALDI and IR-MALDI, additional studies are needed to better understand the similarities and underlying differences in the IR vs. UV desorption/ionization regimes.

Although initially considered a "soft" ionization technique, MALDI generated ions can undergo both prompt and metastable ion fragmentation [8–20]. This is particularly true in UV-MALDI. IR-MALDI, on the other hand, is generally considered [7,21,22] to induce significantly less fragmentation than UV-MALDI, particularly for fragile analytes such as oligonucleotides [23]. The time scale for metastable ion fragmentation in MALDI is such that much of the fragmentation occurs after analyte ions have left the ion source and so is referred to as post-source metastable ion decay (PSD) [8,15,19]. In TOF-MS, this PSD can lead to analyte peak broadening and subsequent decreases in the obtainable resolution for a given analyte [8,15]. In reflectron-based TOF-MS instruments, PSD also often leads to significant ion signal losses and a decrease in sensitivity, especially for larger m/z analytes. PSD of MALDI generated ions can also be useful as an analytical tool for the sequencing of peptides and proteins when reflectron TOF-MS [9–14] is combined with stepped kinetic energy scanning of the ion mirror or with TOF/TOF based mass spectrometers.

* Corresponding author at: Department of Chemistry and Biochemistry, Utah State University, UMC 0300, Logan, UT 84322-0300, United States.
Tel.: +1 435 797 0545; fax: +1 435 797 3390.
E-mail address: bob.brown@usu.edu (R.S. Brown).

1387-3806/$ – see front matter © 2008 Elsevier B.V. All rights reserved.
doi:10.1016/j.ijms.2008.08.021

There are many factors that play a role in the amount of PSD that occurs in MALDI. These include: the matrix that is utilized [15,16], the laser fluence to which the sample is exposed [16], and the ion source extraction conditions that are employed [20]. The amount of PSD an analyte ion undergoes is one measure of the level of ion activation that occurs in a given ionization process. Ion activation levels can provide an indirect measure of the processes occurring during MALDI. Numerous examples can be found in the literature [21,24,25] where IR-MALDI ionization of peptides, proteins and oligonucleotides are shown to produce significantly less fragmentation than ions produced using UV desorption wavelengths. The comparisons between UV and IR based MALDI is further complicated in that, in some studies, significantly different experimental parameters (in addition to the desorption wavelength) are employed. Often, different matrices are utilized that are optimized for the different wavelengths being studied, making direct comparisons difficult since the matrix itself often plays a significant role in the level of ion activation during MALDI [26,27].

It has been noted by several groups [28–32] that when certain matrices are used for IR-MALDI (near ≈3 μm), that the best MALDI spectra are produced at wavelengths that are significantly blue shifted from the observed spectral absorption maximum of the matrix. In some cases this blue shift can be large enough that little or no absorption is observed in conventional infrared spectra of the matrix. This blue shift also corresponds to a minimum in the energy required for desorption. For the majority of the common hydroxy substituted matrices that are used in the present studies, this optimum is observed around 2.82–2.83 μm. Several possible explanations for this phenomenon have been proposed including: contributions to the absorption from surface or interstitial molecules, low levels of residual solvent (water) in the matrix crystals or weakly hydrogen bonded hydroxyl (OH) groups. In an effort to better understand this phenomenon, we have examined the levels of PSD that occur in peptides and proteins that are analyzed by both IR-MALDI at wavelengths near 3 μm and UV-MALDI (337 nm). Common hydroxy substituted UV-MALDI matrices are employed and a gridless deceleration stage coupled to a linear TOF-MS instrument was used to measure the levels of PSD ion fragmentation of model proteins and peptides.

2. Experimental

The time-of-flight mass spectrometer (TOF-MS) used in these studies is a linear geometry instrument that is similar in its basic design to a previously described instrument [33]. A schematic drawing of the instrument's overall design is shown in Fig. 1. In the current instrument, the ion source chamber has two laser ports equipped with appropriate windows and optics (fused silica for the UV and calcium fluoride for the IR) to simultaneously accommodate both an IR and UV laser beam.

2.1. UV laser

A nitrogen laser (Model 79110, Oriel Instruments, Stratford, CT) operating at 337 nm and producing 5 ns pulses was employed for all of the described UV-MALDI studies. The amount of energy employed is controlled using a continuously adjustable variable transmission neutral density filter.

2.2. IR laser

A neodymium-doped yttrium aluminum garnet (Nd:YAG) laser-pumped optical parametric oscillator (OPO) operating in the mid-IR was employed for all of the described IR-MALDI studies. A Surelite I-10 (Continuum, Santa Clara, CA) is used as the pump laser for a custom-built potassium titanyl phosphate (KTP) based OPO (LaserVision, Bellevue, WA). The specific wavelength of the idler beam output of the OPO is adjusted via angle tuning of the KTP crystal. Pump and signal beam outputs of the OPO are eliminated using an appropriate polarizer consisting of a stack of silicon plates mounted at Brewster's angle relative to the OPO output beam. The polarizer only allows the idler beam (which in the current design can be angle tuned from 3.00 to 2.13 μm) to be transmitted and blocks the perpendicularly polarized output of the signal and residual pump beams also exiting the OPO.

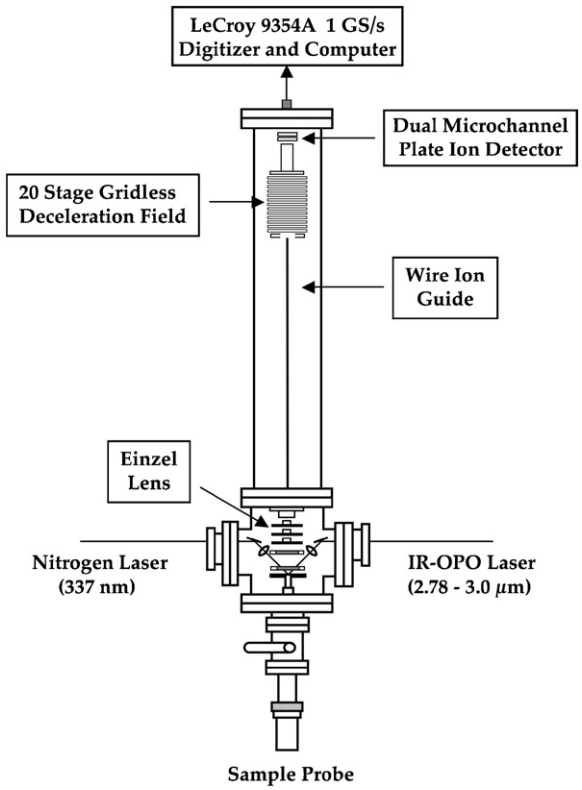

Fig. 1. Diagram of the linear TOF-MS instrument with ion deceleration stage that is used for PSD analysis.

Gross energy attenuation of the idler beam is achieved by utilizing a germanium window in the beam path (resulting in significant reflection losses due to germanium's high refractive). Since germanium does not transmit below 2.0 μm, it also serves as a final optical filter and absorbs any residual signal or pump beam photons that might remain in the output beam after the initial polarizer. The temporal output pulse of the OPO is 4–5 ns. The typical output beam energy required for performing IR-MALDI experiments is dependent on the analyte, matrix and desorption wavelength that is employed. Typical OPO output energies employed for IR-MALDI with the system described range from 0.15 to 1.5 mJ (measured at the entrance of the vacuum chamber's IR window).

Typical spot sizes of the focused beam at the sample are approximately 150 μm × 250 μm for the UV laser and 250 μm × 350 μm for the OPO. For the experiments reported here (both UV-MALDI and IR-MALDI), the photon beam energies were adjusted experimentally for a given matrix to levels just above threshold irradiance, where consistent and stable analyte ion signals were observed. The angle of incidence that both the UV and IR beams hit the sample surface is 60° relative to the surface plane.

Unless otherwise specified, all MALDI-generated mass spectra presented were acquired under delayed ion extraction conditions using an ion source bias voltage of 18 kV (see Fig. 1). Ion extraction

Table 1
Relative[a] PSD levels of ubiquitin in various matrices analyzed by UV-MALDI (337 nm) and IR-MALDI (2.83 μm)

Matrix	PSD levels	
	UV-MALDI	IR-MALDI
α-Cyano-4-hydroxycinnamic acid	15 ± 2	30 ± 5
Caffeic acid	4 ± 1	13 ± 2
Sinapinic acid	3 ± 1	10 ± 1
2,5-Dihydroxybenzoic acid	2 ± 0	8 ± 2
Ferulic acid	<1	4 ± 0

[a] (Neutral peak height)/(Stable ion peak height) × 100.

delay times of 400–800 ns were used and the pulsed extraction voltage was adjusted to optimize the mass resolution for specific delay times and analyte size.

2.3. PSD studies

Temporal separation of the various PSD species was accomplished using a gridless deceleration stage (see Fig. 1). This deceleration stage consisted of a grounded entrance electrode (2.3 mm thick, 20.1 mm radial opening), 19 identical decelerating electrodes (2.3 mm thick, 63.7 mm radial opening), and an elongated exit electrode (129 mm long, 28.5 mm opening). Each of the electrodes was spaced 9.3 mm apart. The decelerating electrodes were electrically connected in series using 10 MΩ resistors. A variable decelerating voltage (5 kV, except where noted in the text) was applied to the exit electrode. This produces a linear voltage drop (5% of the applied voltage at each decelerating electrode) across the ion deceleration stage. The decelerating stage was positioned at the end of the field-free drift region with its exit about 25 mm from the detector surface. For the PSD studies described, an einzel lens and two steering electrodes were used to focus ions through the deceleration stage and onto the ion detector. The wire ion guide normally used for improved ion transmission was grounded for PSD measurements. For the relative PSD levels reported in Tables 1–3, between three and nine replicate deceleration spectra were collected for each wavelength reported. Individual deceleration spectra represent the ensemble average of the ion signal from 20 to 50 laser pulses focused onto the same sample surface.

2.4. MALDI sample preparation

All peptides and proteins were purchased from Sigma Chemical Company (St. Louis, MO), Aldrich Chemical Company (Milwaukee, WI), or Calbiochem-Novabiochem International (San Diego, CA) and were used without further purification. Matrices were purchased from Sigma Chemical Company (St. Louis, MO) or Aldrich Chemical Company (Milwaukee, WI) and were purified by sublimation and recrystallization from a 1:1 mixture of water and acetonitrile. Matrix solutions were prepared to a final concentration of 50 mM with a 1:1 ratio of 0.1% trifluoroacetic acid (aqueous) and acetonitrile. Ten microlitre of analyte solution and 100 μL of matrix solution were mixed to give a solution with concentrations of 9 μM analyte and 45 mM matrix (5000:1 matrix-to-analyte ratio). 2 μL of this final solution was deposited on the sample target (3 mm diameter) and allowed to air dry.

Table 2
Relative[a] PSD levels of various analytes in MALDI using α-cyano-4-hydroxycinnamic acid as a matrix

Analyte	PSD levels			
	337 nm	2.83 μm	2.86 μm	2.89 μm
Insulin chain B	21 ± 3	20 ± 2	13 ± 1	10 ± 2
Insulin	4 ± 0.3	7 ± 1	3 ± 1	2 ± 1
Ubiquitin	15 ± 2	30 ± 5	11 ± 1	9 ± 1
Cytochrome *c*	9 ± 3	22 ± 3	8 ± 1	3 ± 1
Lactalbumin	6 ± 0.3	20 ± 3	7 ± 3	3 ± 0.4

[a] (Neutral peak height)/(Stable ion peak height) × 100.

Table 3
Relative[a] PSD levels of ubiquitin in various matrices analyzed by UV-MALDI and IR-MALDI at varying wavelengths

Matrix	PSD levels			
	337 nm	2.83 μm	2.86 μm	2.89 μm
α-CN-4-OH C.A.	15 ± 2	30 ± 5	11 ± 1	9 ± 1
Caffeic acid	4 ± 1	13 ± 2	7 ± 2	3 ± 1
Ferulic acid	<1	4 ± 1	<1	<1
Sinapinic acid	3 ± 1	10 ± 1	4 ± 1	<1
α-Phenyl-4-OH C.A.	2 ± 1	11 ± 1	4 ± 1	<1
2,5-OH B.A.	2 ± 1	8 ± 2	2 ± 1	<1
Vanillic acid	N/D[b]	<1	<1	<1
2,4-OH B.A.	N/D[b]	3 ± 1	<1	<1
4-OH B.A.	N/D[b]	<1	<1	<1
2,2′,4,4′-OH B.P.	22 ± 5	12 ± 2	7 ± 2	N/D
	PSD levels			
	2.90 μm	2.94 μm		2.96 μm
Fumaric acid[c]	<1	<1		<1

C.A., cinnamic acid; B.A., benzoic acid; B.P., benzophenone; OH, hydroxy; N/D, not determined.
[a] (Neutral peak height)/(Stable ion peak height) × 100.
[b] This matrix produces no analyte signal in UV-MALDI (337 nm).
[c] This matrix does not produce any analyte signal in UV-MALDI (337 nm) or in IR-MALDI at desorption wavelengths <2.90 μm.

2.5. Infrared absorption of matrices

Infrared absorption spectra for selected matrices were collected from samples prepared as KBr pellets (2.5% matrix by weight) utilizing a Mattson Instrument's Galaxy series FTIR spectrometer.

3. Results and discussion

3.1. IR-MALDI desorption wavelength effects

As noted in the introduction, the optimal desorption wavelength observed experimentally in IR-MALDI is significantly blue-shifted relative to the infrared absorption maximum of the matrix observed in a conventional infrared spectrum. This is especially true for the various hydroxy-substituted aromatic compounds that are the most commonly employed matrices for UV-MALDI. Examples of the infrared absorption spectra (2.6–3.2 μm) of several of these common UV-MALDI matrices are presented in Fig. 2. These compounds are also effective as matrices for IR-MALDI. As can be seen in the infrared absorption spectra, the absorption maxima for these matrices generally occur at wavelengths of 2.9 μm or higher. Infrared absorption by the matrix decreases steadily as the wavelength is shortened to 2.8 μm, where it often approaches zero absorbance. The trend in IR-MALDI analyte ion signal vs. desorption wavelength that is observed experimentally is the exact opposite of the bulk matrix absorption trend. Fig. 3 shows IR-MALDI mass spectra produced for a sample of cytochrome *c* in a caffeic acid matrix using various wavelengths (2.78–2.86 μm) and constant laser energy for desorption. Each of the mass spectra represent the sum of the ion signal generated from 100 lasers pulses. In order to be able to effectively observe the low *m*/*z* matrix ion signal levels while avoiding detector saturation effects, a discrete dynode electron multiplier detector (model 119 EM, Thorn EMI) was substituted for the normal MCP ion detector for these measurements.

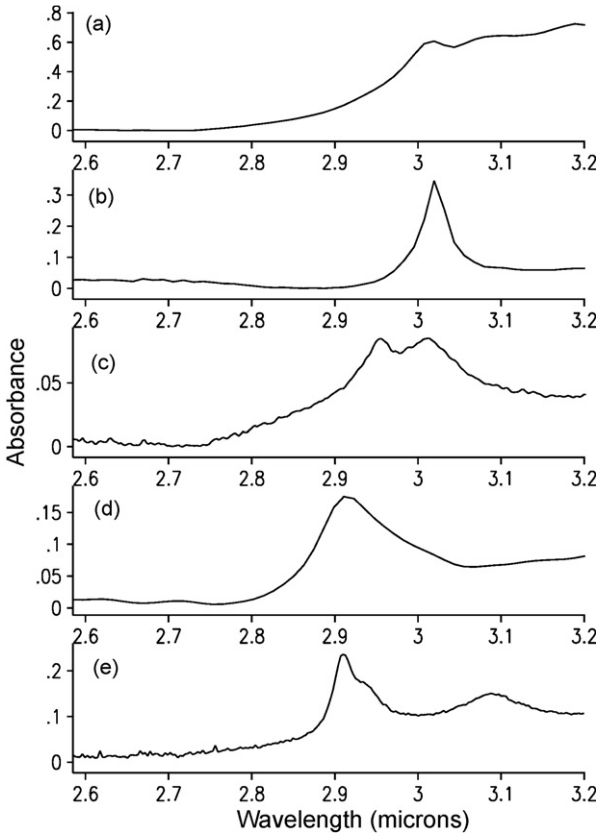

Fig. 2. IR absorbance spectra of (a) 2,5-dihydroxybenzoic acid, (b) α-cyano-4-hydroxycinnamic acid, (c) sinapinic acid, (d) ferulic acid and (e) caffeic acid. Samples were prepared as KBr pellets for FT-IR analysis.

Based upon UV-MALDI behavior, it would be expected that overall ion signal levels would increase as the wavelength used for desorption is increased toward the matrix absorption maximum. However, analyte ion signal yield maximizes at around 2.82 μm and decreases at higher or lower desorption wavelength. The pulse-to-pulse stability of the analyte ion signal also follows this trend and maximizes at 2.82 μm. This was determined by counting the number of individual laser pulses at a given wavelength (out of 100 total laser pulses co-added for each mass spectrum) that resulted in a singly protonated analyte ion signal that was at least 10% of the overall average analyte ion intensity (values noted on each spectrum). Also, the overall intensity of low m/z matrix ions that is observed increases as the wavelength for desorption is changed toward the bulk infrared absorption maximum of the matrix. The trends exhibited in Fig. 3 were observed for all of the aromatic hydroxy-substituted matrices we have examined to date, although the specific optimum wavelength varies for different matrices. In order to better understand the nature of this blue shifted desorption optimum, we have looked at post-source ion decay levels as a function of infrared desorption wavelength as a probe of energy deposition in IR-MALDI.

3.2. Instrument optimization

3.2.1. Ion and neutral transmission

The initial instrument design utilized a wire ion guide [33] to efficiently transfer ions from the source to the detector. However, given the significant radial motion of the ions around the ion guide axis in this type of ion focusing system, significant levels of the neutral metastable fragments produced in PSD are lost in the field-free drift region of the instrument. In order to improve the transmission of the neutral PSD species, an alternative means of ion focusing was utilized. An einzel ion lens was incorporated into the ion source

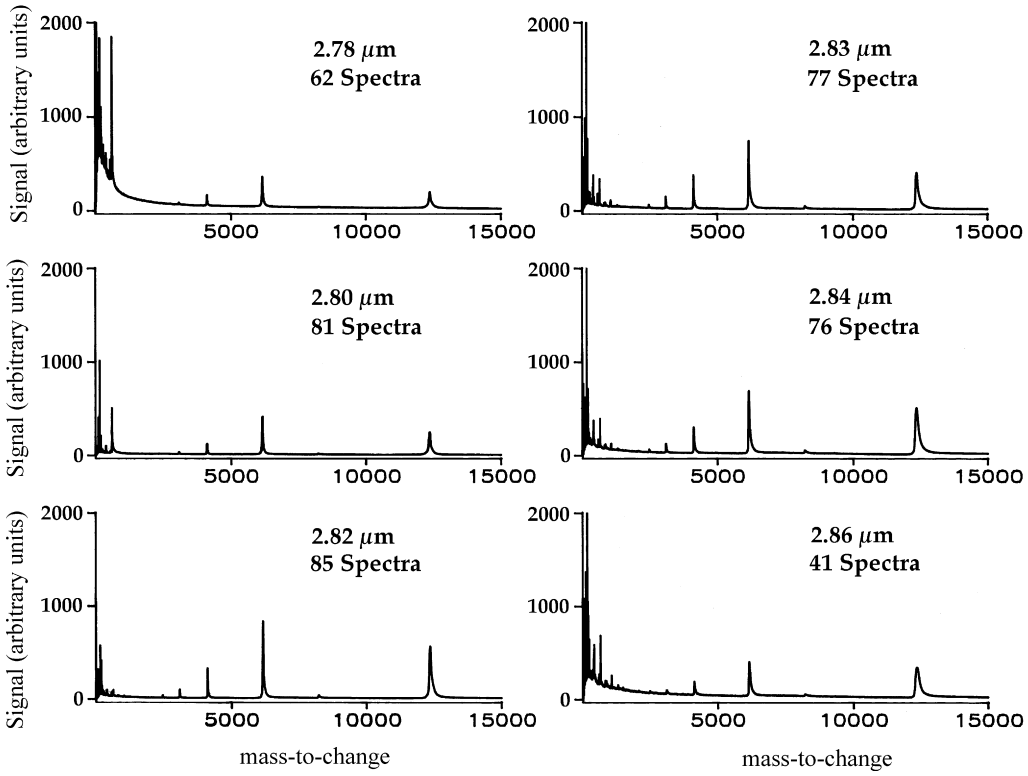

Fig. 3. IR-MALDI spectra of cytochrome *c* in caffeic acid utilizing the indicated wavelength and constant energy. Number of individual spectra with at least 10% of the average analyte ion intensity out of the 100 total collected for co-addition is also indicated for each wavelength.

and the existing ion guide was grounded. By using an einzel lens placed close to the ion source of the mass spectrometer, the focusing electric fields are applied before significant amounts of PSD can occur. By focusing the precursor ions in the ion source, both charged and neutral PSD products that subsequently formed in the field-free drift region will remain focused onto the ion detector and will be detected. A significant increase in the relative level of neutral PSD products was observed using this instrument geometry and all studies reported here utilized this modified geometry.

3.2.2. Ion deceleration stage

If an analyte ion undergoes post-source decay, it fragments in the flight tube of the instrument, losing mass but maintaining a constant velocity in the absence of any applied electrostatic field. If no post-source electrostatic fields are present in the flight path before the PSD products reach the ion detector, then all metastable-generated fragments (charged and neutral) arrive at the detector at essentially the same time as the stable ions that did not fragment. In such a design (i.e., linear TOF-MS), post-source ion decay effects are not observed except perhaps for some minor peak broadening due to the final acceleration field present at the ion detector. The early pioneering PSD studies by Spengler and Kauffman [15,18] utilized an electrostatic deceleration stage placed before the ion detector. This allowed temporal separation of stable analyte ions, ion fragments, and neutral fragments that could be distinguished in the resulting decelerated MALDI time-of-flight spectra. The deceleration stage utilized by Spengler and Kauffman generally included a wire grid electrode at the exit of the deceleration stage. The use of an exit grid produced flat electric field potentials within the deceleration stage that minimized defocusing of the ion beam. A problem with this design was the formation of secondary ions due to collision with the exit grid that complicated the resulting deceleration spectra. To prevent this, the design of the deceleration stage used in the current studies differs from the earlier Spengler and Kauffman design. The exit grid was replaced with an elongated tube electrode. Simion 6 based electrostatic potential models of this gridless ion deceleration stage show that it provides almost as flat potential fields within the deceleration stage as is observed in a deceleration stage with an exit grid. This gridless design eliminates the secondary ion signals in the resulting deceleration spectra. It also provides additional time-of-flight dispersion of the PSD species and stable precursors in the field-free region of the elongated exit electrode. This allowed a lower deceleration voltage to be employed which results in fewer metastable ion fragments being lost due to reflection by the deceleration stage.

3.2.3. Deceleration voltage

The potential used for ion deceleration needs to be optimized for PSD studies. In a pass through ion deceleration stage, some fragment ions will be lost due to reflection by the deceleration stage. Ions that have lost enough kinetic energy due to fragmentation will be reflected as in a conventional ion mirror. Ions with sufficient kinetic energy will be slowed but will exit the deceleration stage and be reaccelerated to the detector. While wishing to minimize reflection losses, a sufficient deceleration potential must be applied to achieve temporal separation of the PSD species. Fig. 4 shows the effect of various deceleration field strengths on UV-MALDI generated ubiquitin ions accelerated from the ion source at 20 kV. The data from Fig. 4 demonstrate that a modest deceleration field, combined with the short field-free drift region of the tube electrode, is sufficient to effectively separate the intact analyte ions (stable $[M+H]^+$) from the neutral metastable fragments (N). Less well resolved are the metastable fragment ions of various m/z (labeled F^+) that are broadly dispersed by the deceleration stage. A 5 kV deceleration field was chosen for subsequent ion deceleration experiments, as it was found to produce sufficient dispersion in the resulting deceleration spectra while minimizing metastable fragment ion losses due to total ion reflection.

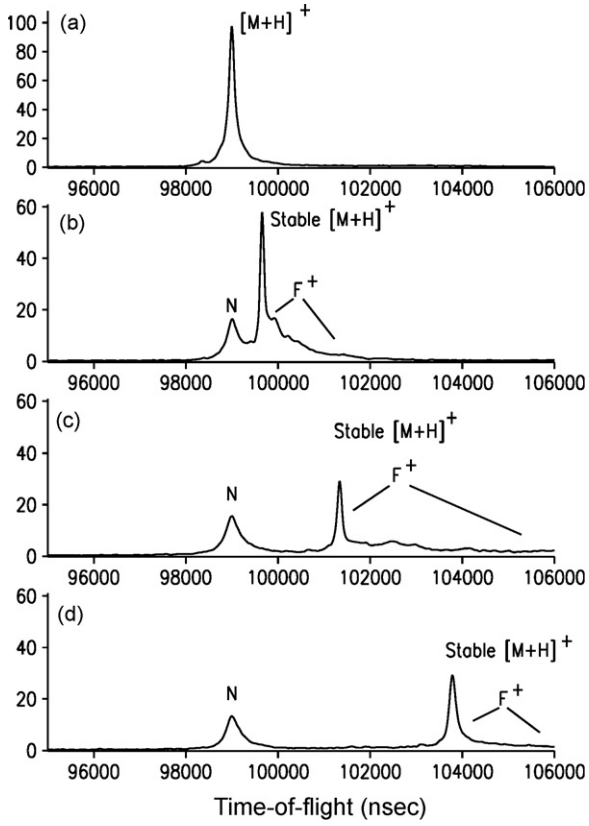

Fig. 4. UV-MALDI spectra of ubiquitin in α-cyano-4-hydroxycinnamic acid. (a) No deceleration, (b) 2 kV deceleration, (c) 6 kV deceleration and (d) 10 kV deceleration. Source acceleration = 20 kV.

3.2.4. Laser energy effects

One experimental parameter that is known to significantly affect the amount of PSD that occurs in UV-MALDI is the laser energy that is employed [16]. Generally, as the laser fluence is increased above the threshold level for ion production, increasingly higher levels of PSD are observed. This effect is easily observed in deceleration time-of-flight spectra produced using the described ion deceleration stage. Fig. 5 shows several deceleration time-of-flight spectra obtained for a sample of ubiquitin prepared in a matrix of α-cyano-4-hydroxycinnamic acid and desorbed (337 nm) using different laser fluences. The spectrum in Fig. 5a was produced using a laser energy level (measured after laser attenuation but before entering the ion source) just above the threshold for successful and sustained ion production. Although changes in the intensity of the fragment ion species (labeled F^+) can easily be discerned as the energy is increased by about 50% (Fig. 5c), more striking is the change in intensity of the well-resolved neutral signals (labeled N) that are observed. As a simple means for quantifying the relative extent of PSD that is occurring in an experiment, the neutral peak's intensity is expressed as a percentage of the stable singly protonated precursor's ($[M+H]^+$) intensity. This percentage is used in subsequent discussions as a measure of the relative level of PSD that is occurring in an experiment. It should be noted that because the peak width of the neutral metastable species are somewhat wider than the stable protonated ion signals, using peak heights instead of areas will tend to underestimate the absolute level of PSD. It does, however, avoid the difficulty in accurately integrating

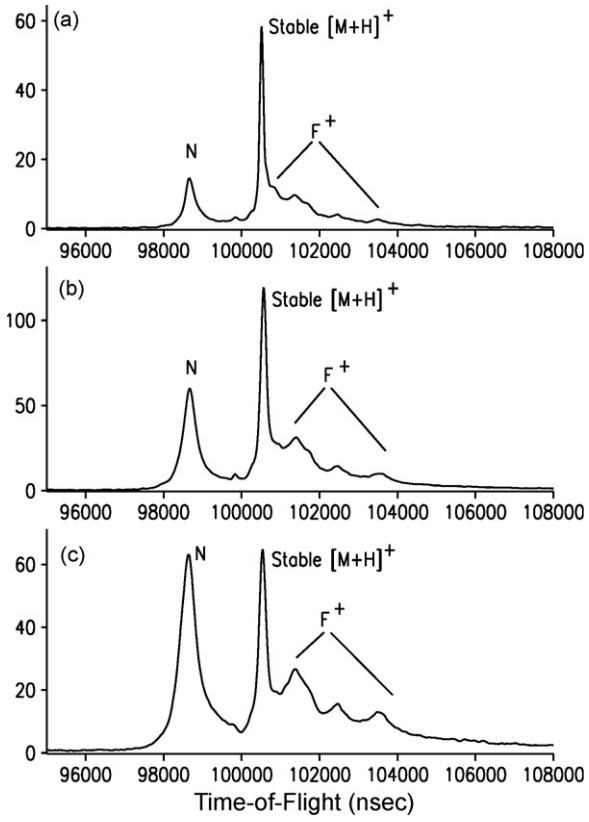

Fig. 5. UV-MALDI spectra of ubiquitin in a-cyano-4-hydroxycinnamic acid at laser energies of (a) 8.5 μJ (near desorption threshold), (b) 10 μJ and (c) 12.5 μJ. Deceleration voltage = 5 kV.

the stable protonated ion signals that occurs due to the overlapping metastable fragment ion signals on the high time-of-flight side of the stable singly protonated ion peaks.

The specific laser energy employed for MALDI is an important parameter to control if meaningful comparisons are to be made with respect to the levels of PSD observed in an experiment. Since the absolute energy required for UV-MALDI and IR-MALDI are significantly different and also matrix dependent, it was decided that relative, rather than absolute energy level effects would be studied. For both the UV-MALDI and IR-MALDI studies reported here, the laser energy employed was adjusted to a level above threshold irradiance that produced analytically useful ion signals for each matrix examined. For the wavelength dependent IR-MALDI studies reported, a single compromise laser energy was chosen for a particular matrix that produced analytically useful ion signals at all of the IR wavelengths examined. This single IR laser energy was than used for all of the PSD vs. wavelength comparisons for a particular matrix. Because these energy levels are comparable to what would be used for producing analytically useful MALDI mass spectra, these studies provide a comparison of the typical levels of PSD that are likely to be observed with a given matrix and wavelength. In order to keep the laser energy employed at different IR wavelengths constant, a calibrated energy attenuator was adjusted to compensate for the small change in the OPO's output energy that occurs as the output wavelength is changed.

In addition to determining the PSD levels observed as a function of IR desorption wavelengths, the level of PSD that occurs in UV-MALDI (337 nm) was also determined for the identical sample preparation. In order to allow meaningful comparisons of the relative UV-MALDI PSD levels, the nitrogen laser's energy was adjusted for each matrix studied so as to produce a singly protonated analyte ion signal intensity equal to that which is observed in the non-decelerated MALDI spectra at the optimal IR desorption wavelength in the corresponding IR-MALDI experiment.

3.3. Post-source ion decay analysis

Because IR-MALDI has generally been categorized as a "softer" ionization method than UV-MALDI, initial expectations were that significantly less PSD would be observed in the case of IR-MALDI when compared to UV-MALDI. This assumption, however, was found to be very dependent on the specific experimental conditions employed for most of the matrices studied. Fig. 6 shows the deceleration MALDI spectra of ubiquitin using caffeic acid as the matrix and analyzed with both UV-MALDI (337 nm) and IR-MALDI (2.82 μm). The IR-MALDI spectrum (Fig. 6b) shows considerably higher levels of both neutral (N) and charged (F^+) metastable decay products than does the equivalent UV-MALDI spectrum (Fig. 6a) for the same sample. With this matrix/analyte combination and infrared desorption wavelength, IR-MALDI induces a higher relative level of ion activation than occurs in UV-MALDI. To explore this unexpected observation further in hopes of better understanding the energy transfer processes occurring during IR-MALDI, additional PSD-MALDI experiments employing a series of common hydroxy substituted matrices were performed using IR desorption near 2.8–2.9 μm. PSD levels for the equivalent UV-MALDI (337 nm) experiments on the same sample are also reported for comparison.

3.3.1. Matrix effects

The matrix utilized in MALDI analysis is known to play a very large role in the amount of PSD observed for a particular analyte species [15–17,20]. Different matrices also exhibit different absorption profiles in the 3 μm region of the infrared that is used

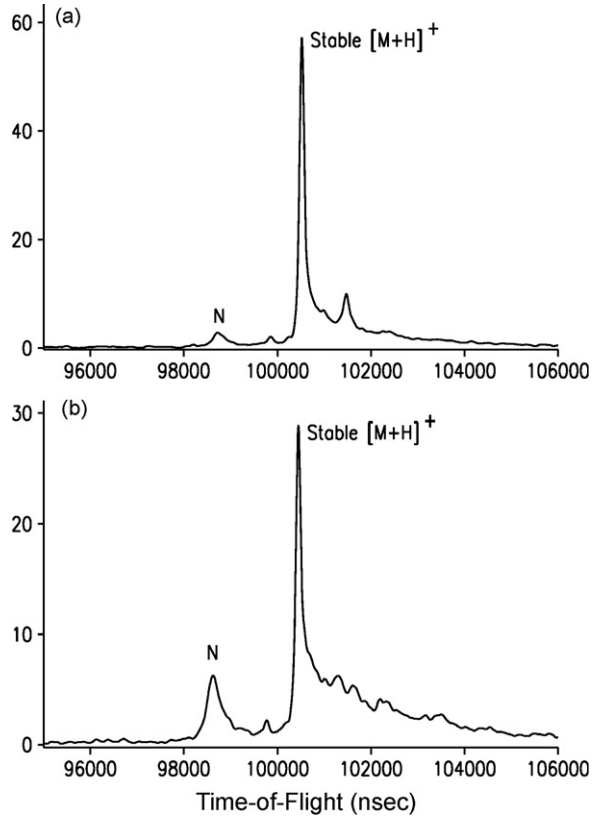

Fig. 6. MALDI spectra of ubiquitin in caffeic acid. (a) UV-MALDI at 337 nm and (b) IR-MALDI at 2.82 μm. Deceleration voltage = 5 kV.

for IR-MALDI. To determine if the high PSD level results for IR-MALDI shown in Fig. 6 were somehow unique for the caffeic acid matrix employed, the levels of PSD induced by a series of common hydroxy substituted MALDI matrices were examined. The matrices whose relative absorption data in the 2.6–3.2 μm region of the infrared was provided in Fig. 2 were chosen for these additional PSD studies. Table 1 shows the relative level of PSD that is induced in ubiquitin by IR-MALDI at 2.83 μm for these hydroxy-substituted matrices. The 2.83 μm desorption wavelength was chosen as this is close to the optimal infrared desorption wavelength for each of these matrices. The UV-MALDI (337 nm) PSD levels are provided for comparison for the same sample preparations. The UV desorption energy was adjusted so as to provide equivalent intensities for the singly protonated ubiquitin ion as was generated in the equivalent IR-MALDI (non-decelerated) spectrum. The results reported are the average PSD levels observed for between three and nine individual deceleration spectra for each matrix and wavelength employed. For these and subsequent comparisons, a numerical representation of the relative amount of PSD which occurs for each experiment is determined by taking the ratio of the neutral metastable ion decay signal height and the stable ion signal height in a particular MALDI deceleration spectrum and expressing this as a percent.

The results in Table 1 indicate that for the case of hydroxy substituted matrices, that IR-MALDI at 2.83 μm appears to be a generally "hotter" ionization method than UV-MALDI at 337 nm for the same matrix. Interestingly, the trend in the level of PSD fragmentation that is observed with the different matrices is generally the same between UV-MALDI and IR-MALDI. Matrices inducing higher levels of PSD in UV-MALDI generally produce similar increases in IR-MALDI. This suggests the possibility that a similar ion activation pathway may be occurring in both UV-MALDI and IR-MALDI. While IR-MALDI at 2.83 μm appears more efficient in driving this activation pathway, small changes in the IR wavelength used for desorption have a significant effect on the extent of ion activation. As is shown below, as the desorption wavelength is shifted to longer IR wavelength (while the laser energy is held constant), less PSD is actually observed despite an increase in bulk matrix absorption as evidenced in the infrared absorption spectra of Fig. 2.

3.3.2. IR-MALDI wavelength effects

Only slight changes in the IR wavelength used for desorption, a few tenths of a micron or less, can dramatically change the amount of PSD observed in an IR-MALDI spectrum. Fig. 7 shows comparative ion deceleration spectra using α-cyano-4-hydroxycinnamic acid as the matrix for both UV-MALDI at 337 nm and IR-MALDI at three different IR wavelengths (2.83, 2.89 and 2.95 μm). At the two longer IR wavelengths, the amounts of PSD observed in the ion deceleration spectra are well below the level observed in the UV-MALDI spectrum. At the shorter 2.83 μm desorption wavelength, the level of PSD is greater than what is observed in the reference UV-MALDI PSD spectrum. This dependence of the PSD level on the IR desorption wavelength has been observed consistently in all of the hydroxy substituted matrices and analytes that were studied. It appears to be a general trend for this class of matrix. In general, IR-MALDI spectra obtained at wavelengths shorter than about 2.85 μm typically produced more PSD than was observed using UV-MALDI when UV and IR laser energies were set to produce comparable levels of protonated ion signals.

To demonstrate that the trend observed in the level of PSD that is occurring is not specific to ubiquitin, Table 2 compares the relative levels of PSD observed using α-cyano-4-hydroxycinnamic acid with various analytes and desorption wavelengths. All of the analytes examined showed the same trend of an increase in observed PSD levels as the desorption wavelength was changed to shorter IR

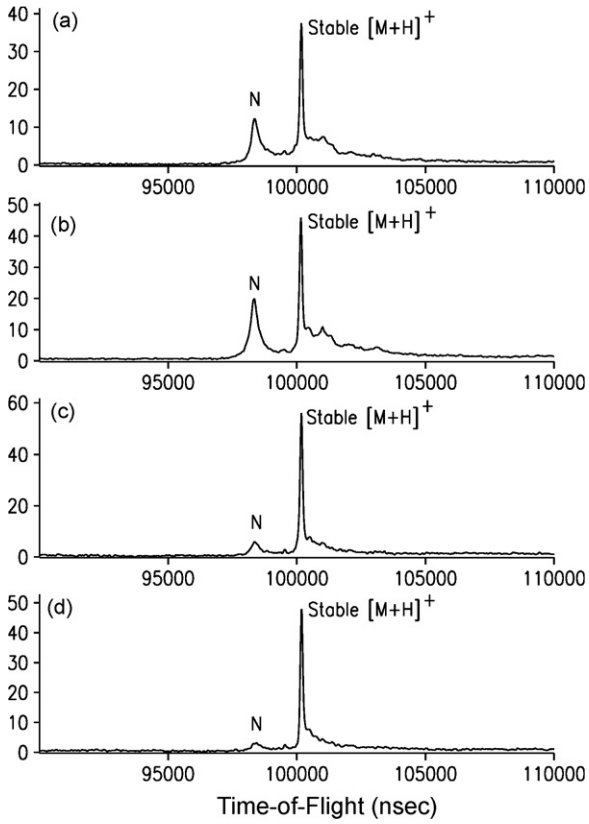

Fig. 7. UV-MALDI and IR-MALDI spectra of ubiquitin in α-cyano-4-hydroxy cinnamic acid. Wavelength (a) 337 nm, (b) 2.83 μm, (c) 2.89 μm and (d) 2.95 μm. Deceleration voltage = 5 kV.

wavelengths. While the α-cyano-4-hydroxycinnamic acid matrix nicely demonstrates these trends due to the higher overall levels of PSD that result from its use, the trends described are not unique to this MALDI matrix. Table 3 summarizes the relative amounts of PSD metastable ion decay that occurs in ubiquitin using a range of MALDI matrices and desorption wavelengths. For all of the hydroxy substituted matrices studied in Table 3, the amount of measurable PSD metastable ion decay increases as the IR desorption wavelength is adjusted to shorter wavelengths. Beyond about 2.90 μm for most of the matrices examined, little PSD is observed. Results using fumaric acid is also included to show the low levels of PSD observed in IR-MALDI using non-hydroxy substituted matrices. Note also that without the hydroxy group, no MALDI signal is generated using an IR wavelength below 2.90 μm.

3.3.3. Collisional stabilization effects

One factor that could account for the decrease in analyte ion activation observed at longer IR wavelengths is improved collisional cooling of analyte ions in the desorption plume. Because of the generally higher bulk absorption of the matrices studied at longer IR wavelengths, significant differences in the amount of ablated material occurs over the IR wavelength range being studied. The higher ablation levels at the longer IR desorption wavelengths should result in a denser initial desorption plume. Higher levels of low energy collisions occurring during initial plume expansion (and prior to the application of the delayed extraction acceleration) could result in more efficient analyte ion cooling and therefore less analyte ion activation. It should be noted that the lower ablation level that is observed at shorter IR desorption wavelengths is relative to the ablation levels at the longer IR desorption wavelengths studied. Ablation levels for all of the IR desorption wavelength

studied (3 μm IR region) are significantly higher than the levels observed in UV-MALDI.

If the elevated level of ablation observed using longer IR wavelengths leads to a denser initial plume that increases the collisional cooling (and therefore lowers ion activation) of analyte ions under delayed ion extraction conditions, similar experiments employing continuous ion extraction might be expected to show a relative increase in PSD formation at longer IR desorption wavelengths. With an initial denser desorption plume and no delay period to allow for plume expansion before ion acceleration, more high-energy collisions between analyte ions and neutrals would be expected. This would lead to an increase in analyte ion (collisional) activation and increased PSD levels at longer IR desorption wavelengths.

Fig. 8 shows MALDI ion deceleration spectra of ubiquitin in α-cyano-4-hydroxycinnamic acid obtained using continuous ion extraction. As expected, the overall PSD levels using continuous ion extraction are much higher than were observed with delayed ion extraction (see Fig. 7) at all desorption wavelengths. However, the same trend in PSD is observed in both cases (i.e., PSD levels decrease with longer IR desorption wavelength). Based upon the relative levels of PSD observed, ion activation appears to increase roughly equally when switching to continuous ion extraction at each of the desorption wavelengths examined. This is presumably due to additional collisional activation. Since little relative change in PSD levels with IR desorption wavelength is observed when switching to continuous ion extraction, this suggests that plume densities differences at the various IR desorption wavelengths may not be large. This would than preclude significant additional collisional cooling at the longer IR desorption wavelengths. If additional collisional cooling is not stabilizing analytes desorbed at the longer IR wavelengths studied, another mechanism is needed to explain the higher ion activation observed at the shorter IR desorption wavelengths. This would mean another ion activation process is occurring in the IR-MALDI and not in the UV-MALDI experiments.

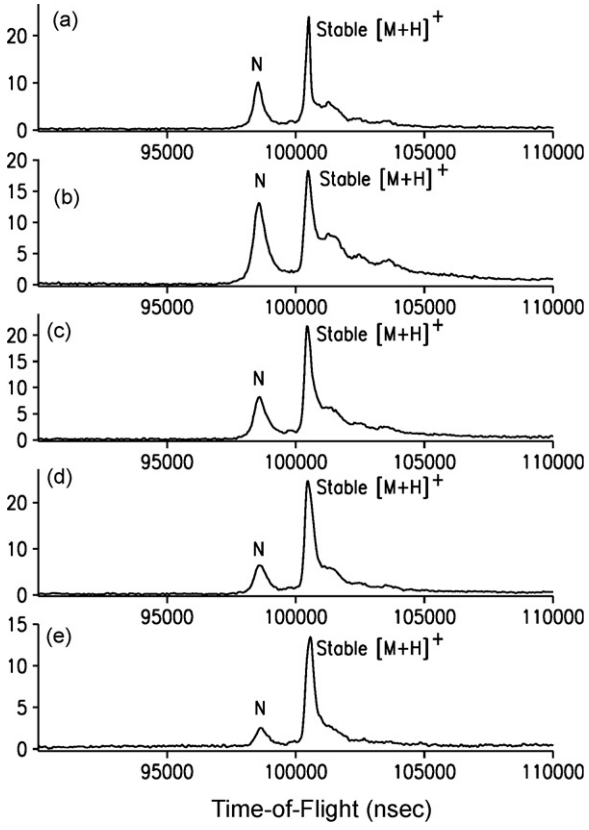

Fig. 8. PSD MALDI spectra of ubiquitin in α-cyano-4-hydroxycinnamic acid. (a) 337 nm, (b) 2.83 μm, (c) 2.86 μm, (d) 2.89 μm and (e) 2.92 μm. Continuous ion extraction voltage = 19.2 kV. Deceleration voltage = 5 kV.

4. Conclusions

Relative PSD levels in IR-MALDI can be highly dependent upon the desorption wavelength employed. For hydroxy substituted matrices, although optimum analyte ion signal relative to matrix background is generated at shorter wavelengths (typically 2.8–2.83 μm), PSD levels for analytes desorbed at these wavelengths can be as high or higher than in UV-MALDI for the same matrix. At longer IR wavelengths (typically above 2.90 μm) where bulk matrix absorption is much higher, little or no PSD is observed, consistent with most reports in the literature (many employing the fixed 2.94 μm output of the Er:YAG laser). Given these results, the generally accepted characterization of IR-MALDI as an overall "softer" ionization method relative to UV-MALDI needs to be reconsidered, at least when hydroxy substituted matrices are employed.

At longer IR wavelengths (>2.86 μm), more matrix material is physically ablated (based upon visual inspection of samples), relative to the shorter IR wavelengths studied, when the desorption energy is held constant as in the current studies. This is consistent with the trend in the bulk matrix absorption spectra shown in Fig. 2. Also, significantly increased levels of larger matrix cluster ions are observed in the MALDI mass spectra generated using certain matrices (i.e., vanillic acid, data not shown) using longer IR desorption wavelengths (typically > 2.90 μm). This suggests that some enhanced collisional stabilization could be occurring at the longer IR desorption wavelengths, but it does not appear to explain the high levels of analyte ion activation at shorter IR desorption wavelengths, which can be comparable or even higher than that observed in UV-MALDI. Even at the shortest IR desorption wavelengths examined, significantly higher ablation of the sample occurs in IR-MALDI than in UV-MALDI. The results suggest that there is likely an additional ion activation pathway involved in the IR-MALDI experiments.

Direct energy deposition into the analyte may be occurring at the shorter IR wavelengths, leading to the increased ion activation that is observed. It can be speculated that this direct vibrational activation of the analyte might be related to energy absorption via weakened hydrogen bonds between the matrix and analyte in the sample. This would be consistent with the significant blue shift of the optimum desorption wavelength observed with these matrices in IR-MALDI. Significant spectral blue shifts are observed for some –OH absorption stretches in the IR of molecules in an aprotic environment. For example, a strong and sharp absorption band due to a non-hydrogen bonded –OH group is observed at 2.78 μm for phenol when prepared in a solvent of chloroform (data not shown). This is close to the wavelength where the hydroxy substituted matrices studied produce both the best IR-MALDI spectra (at least with linear TOF instruments) and the highest level of PSD. Weakened, instead of non-hydrogen bonded species in the matrix crystals may account for the longer optimal absorption wavelength observed experimentally in IR-MALDI. This could indicate a subset of matrix molecules, or perhaps residual water molecules, are present within the "bulk" matrix, which are absorbing the IR energy at the blue shifted IR wavelength. This could result from differences in the local hydrogen bond environment for these molecules. While producing stronger analyte ion signals and lower matrix background levels in the resulting MALDI mass spectra (due to perhaps improved cluster evaporation as suggested by the Lucky Survivor model) this process may also result in more energy transfer to the analyte, causing higher ion activation levels.

Acknowledgements

This research was supported, in part, by grants from the National Institutes of Health, Divisions of Research Resources (RR05311) and General Medical (GM47914) and with funds provided by Utah State University. This support is gratefully acknowledged.

References

[1] M. Karas, D. Bachmann, U. Bahr, F. Hillenkamp, Int. J. Mass Spectrom. Ion Proc. 78 (1987) 53.
[2] H. Ehring, M. Karas, F. Hillenkamp, Org. Mass Spectrom. 27 (1992) 472.
[3] M. Karas, M. Gliickmann, J. Schafer, J. Mass Spectrom. 35 (2000) 1.
[4] R. Knochenmuss, J. Mass Spectrom. 37 (2002) 867.
[5] R. Knochenmuss, Anal. Chem. 75 (2003) 2199.
[6] K. Dreisewerd, Chem. Rev. 103 (2003) 395.
[7] K. Dreisewerd, S. Berkenkamp, A. Leisner, A. Rohlfing, C. Menzel, Int. J. Mass Spectom. 226 (2003) 189.
[8] B. Spengler, D. Kirsch, R. Kaufmann, Rapid Commun. Mass Spectrom. 5 (1991) 198.
[9] R. Kaufmann, B. Spengler, F. Lutzenkirchen, Rapid Commun. Mass Spectrom. 7 (1993) 902.
[10] B. Spengler, J. Mass Spectrom. 32 (1997) 1019.
[11] P. Chaurand, F. Lutzenkirchen, B. Spengler, J. Am. Soc. Mass Spectrom. 10 (1999) 91.
[12] R.S. Annan, S.A. Carr, Anal. Chem. 68 (1996) 3413.
[13] J. Vinh, D. Loyaux, V. Redeker, J. Rossier, Anal. Chem. 69 (1997) 3979.
[14] M.D. Jones, S.D. Patterson, H.S. Lu, Anal. Chem. 70 (1998) 136.
[15] B. Spengler, D. Kirsch, R. Kaufmann, J. Phys. Chem. 96 (1992) 9678.
[16] T.J.P. Naven, D.J. Harvey, J. Brown, G. Critchley, Rapid Commun. Mass Spectrom. 11 (1997) 1681.
[17] M. Karas, U. Bahr, K. Strupat, F. Hillenkamp, A. Tsarbopoulos, N. Pramanik, Anal. Chem. 67 (1995) 675.
[18] R.S. Brown, J. Feng, D.C. Reiber, Int. J. Mass Spectrom. Ion Proc. 169/170 (1997) 1.
[19] B. Spengler, R. Kaufmann, Analysis 20 (1992) 91.
[20] R. Kaufmann, P. Chaurand, D. Kirsch, B. Spengler, Rapid Commun. Mass Spectrom. 10 (1996) 1199.
[21] W. Zhang, S. Niu, B.T. Chait, J. Am. Soc. Mass Spectrom. 9 (1998) 879.
[22] H.J. Cha, J.H. Moon, M.S. Kim, Rapid Commun. Mass Spectrom. 21 (2007) 1468.
[23] F. Kirpekar, S. Berkenkamp, F. Hillenkamp, Anal. Chem. 71 (1999) 2334.
[24] C. Menzel, S. Berkenkamp, F. Hillenkamp, Rapid Commun. Mass Spectrom. 13 (1999) 26.
[25] S. Berkenkamp, C. Menzel, M. Karas, F. Hillenkamp, Rapid Commun. Mass Spectrom. 11 (1997) 1399.
[26] J. Kampmeier, K. Dreisewerd, M. Schürenberg, K. Strupat, Int. J. Mass Spec. Ion Proc. 169/170 (1997) 31.
[27] K. Strupat, J. Kampmeier, V. Horneffer, Int. J. Mass Spec. Ion Proc. 169/170 (1997) 43.
[28] C. Menzel, K. Dreisewerd, S. Berkenkamp, F. Hillenkamp, Int. J. Mass Spectrom. 207 (2001) 73.
[29] M. Sadeghi, Z. Olumee, X. Tang, A. Vertes, Z.X. Jiang, A.J. Henderson, H.S. Lee, C.R. Prasad, Rapid Commun. Mass Spectrom. 11 (1997) 393.
[30] J.D. Sheffer, K.K. Murray, Rapid. Commun. Mass Spectrom. 12 (1998) 1685.
[31] R. Cramer, F. Hillenkamp, R.F. Haglund, J. Am. Soc. Mass Spectrom. 7 (1996) 1187.
[32] R. Cramer, R.F. Haglund, F. Hillenkamp, Int. J. Mass Spectrom. Ion Process. 169/170 (1997) 51.
[33] R.S. Brown, J.J. Lennon, Anal. Chem. 67 (1995) 1998.